the disaggregation of benthic organisms living in the nearby shallow waters of the Bermuda Platform.

The importance of a possible input of detrital carbonate, originally secreted in shallow water, to the deep sea is supported by our sediment trap results. In the < 63-μm fraction at 667 m of station PB and at all depths at station E, the calcite x-ray diffraction peak exhibited a small high-angle "shoulder" due to the presence of high-magnesium calcite (Fig. 1). This high-magnesium calcite, with 13 mode mole percent $MgCO_3$ [determined from the unit cell and diffraction data of Graf (*4*)] could be derived only from shallow-water benthic organisms since no planktonic organism is known that secretes calcite with such a high magnesium content (*7*, *8*). High-magnesium calcite, along with aragonite, are the characteristic phases secreted by shallow-water calcareous organisms. Even though the trap locations are far from the nearest land (more than 200 km in both cases), there is still evidence of a shallow-water component of the $CaCO_3$ found in the traps. Traps located closer to continental shelves or oceanic islands would most likely show a higher aragonite content. The production rate of aragonite in shallow waters is extremely high (*7*, *9*), and just a small "leak" of shallow-water carbonate to nearby portions of the deep sea by resuspension, horizontal transport, and settling would considerably augment the pelagic flux of biogenic aragonite. There is thus additional evidence for the contention that 12 percent is an absolute minimum value for aragonite sedimentation relative to calcite sedimentation on a worldwide basis.

If aragonite and associated high-magnesium calcite fluxes to the deep sea from oceanic islands and continental shelves are quantitatively significant, then dissolution of this material at depth may constitute an important mechanism for the neutralization of excess anthropogenic CO_2 added to the oceans. This is so because aragonite and high-magnesium calcite are distinctly more soluble than low-magnesium calcite (as found in planktonic foraminifera and coccoliths), and consequently they can dissolve at much shallower depths. If the eroded aragonite and high-magnesium calcite particles are sufficiently small that they settle very slowly, then dissolution during sedimentation may occur at relatively shallow depths, and as a result some anthropogenic CO_2 that has penetrated to these depths may be neutralized. [Evidence for extensive in situ $CaCO_3$ dissolution in the Pacific Ocean has recently been given by Fiadeiro (*10*).] Sediment trap studies conducted near carbonate-rich oceanic islands are needed to test this hypothesis.

ROBERT A. BERNER
Department of Geology and Geophysics, Yale University, New Haven, Connecticut 06520
SUSUMU HONJO
Department of Geology and Geophysics, Woods Hole Oceanographic Institution, Woods Hole, Massachusetts 02543

References and Notes

1. N. R. Andersen and A. Malahoff, Eds., *The Fate of Fossil Fuel CO_2 in the Oceans* (Plenum, New York, 1977); W. S. Broecker, T. Takahashi, H. J. Simpson, T.-H. Peng, *Science* **206**, 409 (1979).
2. R. A. Berner, in *The Fate of Fossil Fuel CO_2 in the Oceans*, N. R. Andersen and A. Malahoff, Eds. (Plenum, New York, 1977), p. 243.
3. S. Honjo, *J. Mar. Res.* **36**, 469 (1978); *ibid.* **38**, 53 (1980).
4. D. L. Graf, *Am. Mineral.* **46**, 1283 (1961).
5. J. W. Morse and R. A. Berner, in *Chemical Modeling in Aqueous Systems*, E. A. Jenne, Ed. (Symposium Series 93, American Chemical Society, Washington, D.C., 1979), p. 499.
6. R. A. Berner, E. K. Berner, R. S. Keir, *Earth Planet. Sci. Lett.* **30**, 169 (1976).
7. J. D. Milliman, *Marine Carbonates* (Springer-Verlag, New York, 1974).
8. H. Lowenstam, personal communication; K. E. Chave, personal communication.
9. A. C. Neumann and L. S. Land, *J. Sediment. Petrol.* **45**, 763 (1968); W. W. Hay and J. R. Southam, in *The Fate of Fossil Fuel CO_2 in the Oceans*, N. R. Andersen and A. Malahoff, Eds. (Plenum, New York, 1977), p. 569.
10. M. Fiadeiro, *Earth Planet. Sci. Lett.* **49**, 499 (1980).
11. Research supported by NSF grant OCE 79-06919 to R.A.B. and grants OCE 77-27004 and OCE 79-25429 to S.H.

2 September 1980; revised 14 November 1980

Retinal Chromophore of Rhodopsin Photoisomerizes Within Picoseconds

Abstract. *A new picosecond resonance Raman technique shows that resonance Raman lines characteristic of a distorted all-*trans *retinal appear within 30 picoseconds after photolysis of rhodopsin or isorhodopsin. This finding suggests that isomerization is nearly complete within picoseconds of the absorption of a photon.*

The light-absorbing molecule in all known visual systems is 11-*cis* retinal, a chromophore derived from all-*trans* retinol (vitamin A) (*1*). Rhodopsin, the photoreceptor pigment in vertebrate retinal rod cells, consists of 11-*cis* retinal bound to opsin, a 38-kilodalton protein. Photoisomerization of this bound retinal chromophore from the 11-*cis* to the all-*trans* form triggers the amplification cascade that leads to a nerve impulse (*2*).

Rhodopsin has a strong absorption peak centered at 500 nm due to its 11-*cis* retinal chromophore (*1*). Absorption of a photon leads to the formation of bathorhodopsin, a photolytic intermediate with a broad absorption band centered at 540 nm (*3*). Picosecond absorption studies have shown that this 540-nm absorption band appears, and the 500-nm rhodopsin absorption band is depleted in less than 6 picoseconds after irradiation (*4*-*6*). The precise structure of this rapidly formed photolytic intermediate has been the subject of controversy. One interpretation is that the chromophore in this intermediate, presumed to be bathorhodopsin, is essentially in the all-*trans* form (*3*, *7*, *8*). However, there has been doubt as to whether the sizable atomic motion required for the photoisomerization of retinal could take place on a picosecond time scale. An alternative hypothesis attributing the formation of bathorhodopsin to a very rapid proton transfer instead of an isomerization has been advanced (*5*).

Resonance Raman spectroscopy can provide valuable information concerning the nature of the primary event in vision. Resonance Raman spectra display vibrations that are coupled to electronic tran-

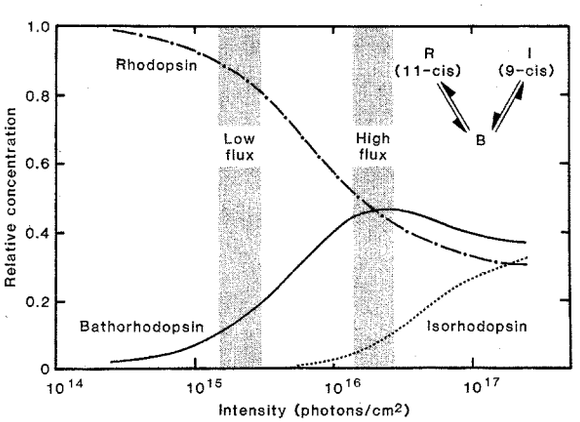

Fig. 1. Relative concentrations of rhodopsin (*R*), bathorhodopsin (*B*), and isorhodopsin (*I*) in the illuminated volume as a function of the intensity of a picosecond light pulse. The proportions of these species were calculated from known absorption cross sections and photoconversion quantum yields (*17*).

0036-8075/81/0227-0942$00.50/0

sitions. Hence, this technique can be more informative than absorption spectroscopy in delineating the detailed conformation of chromophores in macromolecules (*9*). Comparison of the resonance Raman spectra of rhodopsin with those of model retinal compounds has shown that the chromophore in rhodopsin is an undistorted 11-*cis* retinal joined to opsin by a protonated Schiff-base linkage (*10*).

In contrast, bathorhodopsin produced by steady-state illumination of rhodopsin at low temperature displays three low-wave-number lines (853, 874, and 921 cm^{-1}) that are absent from the spectra of all other visual pigments and model compounds studied thus far (*11*). Isotopic and chemical substitution studies have demonstrated that these distinctive lines are produced by out-of-plane vinyl hydrogen motions of $C_{14}H$, $C_{10}H$, and $HC_{11}=C_{12}H$, respectively, and arise from a distorted all-*trans* form of the retinal chromophore (*12, 13*). These low-wave-number lines also appear in the Raman spectrum of bathorhodopsin produced by the photolysis of rhodopsin at room temperature with nanosecond pulses (*14*).

We now report picosecond resonance Raman studies that were designed to ascertain the nature of bathorhodopsin produced within picoseconds of the absorption of a photon. This technique has inherently high temporal as well as structural resolution, as shown by recent picosecond studies of hemoglobin (*15, 16*). Our main aim was to determine whether the low-wave-number lines, a criterion of isomerization, are already present picoseconds after the photolysis of rhodopsin.

The strategy of our experiment was to illuminate flowing samples of rhodopsin with picosecond laser pulses of intensity just sufficient to cause moderate photolysis in the illuminated volume, at a repetition rate high enough to accumulate a sufficient signal from the very weak Raman scattering process. The pulses were generated from a flash-pumped, electrooptically Q-switched, and passively mode-locked Nd:YAG laser operated at 30 pulses per second. A single laser pulse selected from each train of pulses was doubled to 532 nm in an angle phase-matched cesium dihydrogen arsenate crystal. Detergent solutions of purified rhodopsin prepared from bovine retinas were flowed through the illuminated volume at a velocity sufficient to assure a fresh sample volume for each laser pulse. Isorhodopsin, synthesized from opsin and 9-*cis* retinal, was also studied because it is present along with rhodopsin and bathorhodopsin in photostationary steady-state mixtures at low temperature (*3*). The Raman spectra were collected by a double Raman monochromator (Spex 1401) with a cooled photomultiplier (RCA 31034). Laser reference and Raman scattering signals were accumulated on each pulse, and data from unacceptable laser pulses were discarded. Data collection and laser diagnostics were controlled by an LSI-11 computer.

The picosecond laser pulses in our experiment photolyzed the illuminated volume while producing Raman scattering. The calculated relative concentrations of rhodopsin, bathorhodopsin, and isorhodopsin in the illuminated volume as a function of photon flux are shown in Fig. 1. The shaded bands illustrate low-flux and high-flux conditions. At low flux, the illuminated volume contains nearly pure rhodopsin, whereas at high flux, a significant population of bathorhodopsin is produced during a single pulse.

A typical resonance Raman spectrum of rhodopsin obtained with our picosec-

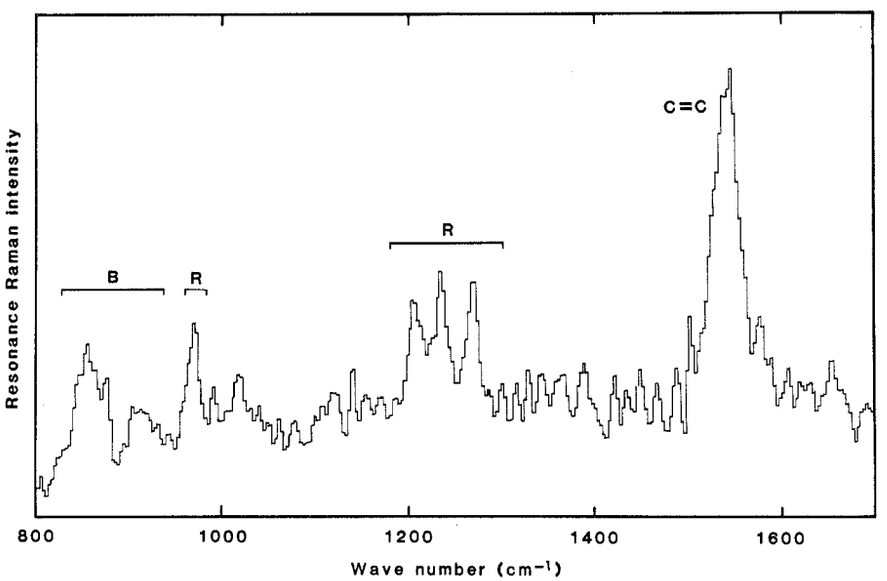

Fig. 2 (left). High-flux resonance Raman spectrum of rhodopsin excited at 532 nm with 30-picosecond pulses. The positions of the distinctive lines of bathorhodopsin are marked by *B* and those of rhodopsin by *R*. The ethylenic region is denoted by C=C. A solution of hydroxylapatite column-purified rhodopsin ($9 \times 10^{-5} M$) in 1 percent Ammonyx LO, 1 m*M* dithiothreitol, 10 m*M* hydroxylamine, and 43 m*M* sodium phosphate, *p*H 7.0, at 4°C was flowed across the illuminated volume, which had a length of 0.2 cm and a diameter of 0.035 cm, at a flow velocity greater than 3 cm/sec. The resolution of the spectrometer was 6 cm^{-1}. The fluorescence background is three times as high as the major peak.

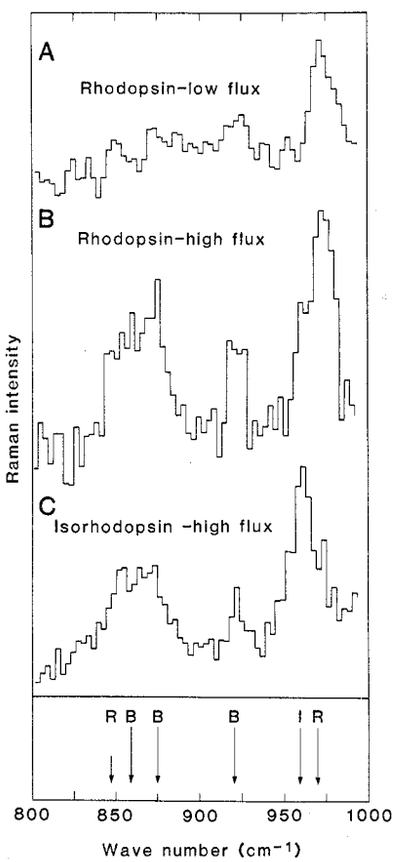

Fig. 3 (right). Resonance Raman spectra of rhodopsin and isorhodopsin excited at 532 nm with 30-picosecond pulses. (A) Low flux spectrum of rhodopsin. (B) High flux spectrum of rhodopsin. (C) High flux spectrum of isorhodopsin. The known positions of rhodopsin (*R*), bathorhodopsin (*B*), and isorhodopsin (*I*) lines (*10, 11*) in this spectral region are marked in the lower part of this figure. The step size was 3 cm^{-1}. Each spectrum is the sum of three scans from 800 to 1000 cm^{-1}, with 256 laser pulses per step in each run. It is interesting to note that the light pulses used to obtain these spectra had a total duration of less than 10^{-5} seconds, compared with 10^{8} seconds spent in designing these experiments and constructing the apparatus.

ond apparatus under high flux conditions is shown in Fig. 2. This spectrum displays bands characteristic of rhodopsin and bathorhodopsin that were previously seen in steady-state resonance Raman spectra. We collected more detailed Raman spectra (Fig. 3) in the region between 800 and 1000 cm^{-1} using both a low photon flux (producing little photoalteration) and a high photon flux (producing moderate photoalteration while avoiding possible nonlinear or saturation effects). The low-flux spectrum of rhodopsin (top curve) contains a major peak that matches the distinctive 971 cm^{-1} line of unphotolyzed rhodopsin. The spectrum observed at higher flux levels (middle curve) exhibits new bands that correspond closely to the distinctive 853, 874, and 921 cm^{-1} bands of bathorhodopsin. This spectrum also exhibits a shoulder at 960 cm^{-1} that probably arises from isorhodopsin molecules produced by the subsequent photolysis of bathorhodopsin during the same 30-picosecond pulse. The high-flux spectrum of isorhodopsin (bottom curve) exhibits similar Raman bands at the bathorhodopsin positions. In addition, the 960 cm^{-1} band characteristic of isorhodopsin in this spectrum has a shoulder near 969 cm^{-1} that is probably due to rhodopsin molecules formed during the pulse.

The appearance of the low-wave-number lines of bathorhodopsin in our 30-picosecond rhodopsin spectrum shows that isomerization from 11-*cis* to a distorted all-*trans* form takes place within picoseconds of the absorption of a photon. Likewise, the picosecond Raman spectrum of photolyzed isorhodopsin shows that isomerization from 9-*cis* to a distorted all-*trans* form is also very rapid. The finding of an isorhodopsin shoulder in the high-flux rhodopsin spectrum, and vice versa, shows that these species can be interconverted in less than 30 picoseconds, probably via a common intermediate—bathorhodopsin. The resonance Raman studies reported here strongly support the hypothesis that the primary event in vision, occurring in times of picoseconds or less, is an isomerization of the retinal chromophore.

GARY HAYWARD
WILLIAM CARLSEN
ANTHONY SIEGMAN
LUBERT STRYER

Department of Applied Physics and *Edward L. Ginzton Laboratory, Stanford University*, and *Department of Structural Biology, Sherman Fairchild Center, Stanford University School of Medicine, Stanford, California 94305*

References and Notes

1. G. Wald, *Science* **162**, 230 (1968).
2. For a review, see W. L. Hubbell and M. D. Bownds, *Annu. Rev. Neurosci.* **2**, 17 (1979).
3. T. Yoshizawa and G. Wald, *Nature (London)* **197**, 1279 (1963); R. Hubbard and A. Kropf, *Proc. Natl. Acad. Sci. U.S.A.* **44**, 130 (1958).
4. G. E. Busch, M. L. Applebury, A. A. Lamola, P. M. Rentzepis, *Proc. Natl. Acad. Sci. U.S.A.* **69**, 2802 (1972).
5. K. Peters, M. Applebury, P. Rentzepis, *ibid.* **74**, 3119 (1977).
6. T. G. Monger, R. R. Alfano, R. H. Callender, *Biophys. J.* **27**, 105 (1979).
7. R. Callender and B. Honig, *Annu. Rev. Biophys. Bioeng.* **6**, 33 (1977).
8. B. Honig, T. Ebrey, R. H. Callender, U. Dinur, M. Ottolenghi, *Proc. Natl. Acad. Sci. U.S.A.* **76**, 2503 (1979).
9. R. Mathies, in *Chemical and Biochemical Applications of Lasers*, C. B. Moore, Ed. (Academic Press, 1979), vol. 4, pp. 55–110.
10. R. Mathies, A. R. Oseroff, L. Stryer, *Proc. Natl. Acad. Sci. U.S.A.* **73**, 1 (1976); R. Mathies, T. D. Freedman, L. Stryer, *J. Mol. Biol.* **109**, 367 (1977).
11. A. R. Oseroff and R. H. Callender, *Biochemistry* **13**, 4243 (1974); B. Aton, A. G. Doukas, D. Narva, R. H. Callender, U. Dinur, B. Honig, *Biophys. J.* **29**, 79 (1980).
12. G. Eyring, B. Curry, R. Mathies, R. Fransen, I. Palings, J. Lugtenburg, *Biochemistry* **19**, 2410 (1980).
13. G. Eyring, B. Curry, R. Mathies, *J. Am. Chem. Soc.* **102**, 5390 (1980).
14. G. Eyring and R. Mathies, *Proc. Natl. Acad. Sci. U.S.A.* **76**, 33 (1979).
15. J. Terner, T. G. Spiro, M. Naguro, M. F. Nicol, M. A. El-Sayed, *J. Am. Chem. Soc.* **102**, 3238 (1980).
16. H. Coppey, H. Tourbez, P. Valat, B. Alpert, *Nature (London)* **284**, 568 (1980).
17. J. B. Hurley, T. G. Ebrey, B. Honig, M. Ottolenghi, *ibid.* **270**, 540 (1977).
18. Supported by grant EY-02387 from the National Eye Institute. We thank S. Slaughter for technical assistance and R. Mathies for discussions.

21 August 1980; revised 21 October 1980

Electrochemical Reduction of Horse Heart Ferricytochrome c at Chemically Derivatized Electrodes

Abstract. *Platinum or gold electrodes derivatized with an* N,N′*-dialkyl-4,4′-bipyridinium reagent can be used to reduce horse heart ferricytochrome c, whereas reduction does not occur at the "naked" electrodes. From 3 to 17.7 millimoles per liter, the reduction of ferricytochrome c is mass transport–limited at electrode potentials more negative than about −0.6 volt against a saturated calomel reference electrode. Data for the photoreduction of ferricytochrome c at derivatized* p*-type silicon photocathodes show directly that the rate of reduction is mass transport–limited. Use of derivatized electrodes may allow convenient manipulation and analysis of biological molecules that do not ordinarily respond at conventional electrodes.*

We report significant enhancement of the rate of electrochemical reduction of horse heart ferricytochrome c [cyt $c_{(ox)}$] by surface derivatization of Au, Pt, or *p*-type Si electrodes with reagent **1**, {*N*,*N*′-bis[3-(trimethoxysilyl)propyl]-4,4′-bipyridinium}dibromide (*1*). The cyt $c_{(ox)}$ gives a negligible response (*2*) at the "naked" (nonderivatized) electrode in the same potential regime. Large biological molecules having an electron transfer function often do not respond at conventional electrodes because the redox center—heme in cyt $c_{(ox)}$—cannot come close enough to the electrode (*3*). Such unresponsive molecules do react with

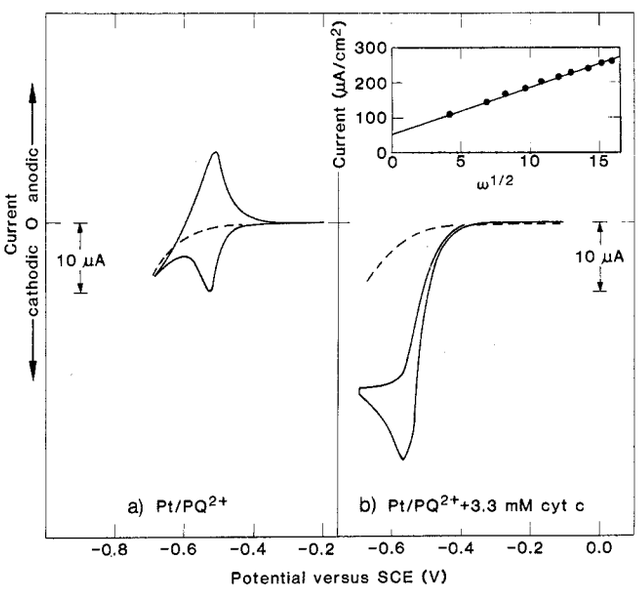

Fig. 1. Cyclic voltammetry of Pt wire electrodes at 5 mV/sec. (a) Scans of electrode (- - -) naked and (——) derivatized (2×10^{-8} mole/cm^2) with **1** in a stirred 1.0*M* $NaClO_4$ solution at *p*H 7.0 (phosphate). (b) Same conditions as in (a) after addition of 3.3 m*M* cyt $c_{(ox)}$. (Inset) Steady-state current at − 0.7 V versus SCE plotted against $\omega^{1/2}$ for a derivatized (2.1×10^{-8} mole/cm^2) rotating Pt disk electrode under the same conditions as in (b). In 1.0*M* KBr electrolyte at *p*H 7 the pretreated, but not derivatized, electrodes show no cyt $c_{(ox)}$ reduction current, but derivatized electrodes in 1.0*M* KBr behave the same way as in 1.0*M* $NaClO_4$, *p*H 7, used here.

0036-8075/81/0227-0944$00.75/0